

# Electric field induced thermal Hall effect of triplons in the quantum dimer magnets $X\text{CuCl}_3$ ( $X = \text{Tl}, \text{K}$ )

Nanse Esaki,<sup>1,\*</sup> Yutaka Akagi,<sup>1</sup> and Hosho Katsura<sup>1,2,3</sup>

<sup>1</sup>*Department of Physics, Graduate School of Science,  
The University of Tokyo, 7-3-1 Hongo, Tokyo 113-0033, Japan*

<sup>2</sup>*Institute for Physics of Intelligence, The University of Tokyo, 7-3-1 Hongo, Tokyo 113-0033, Japan*

<sup>3</sup>*Trans-scale Quantum Science Institute, The University of Tokyo, 7-3-1, Hongo, Tokyo 113-0033, Japan*

We propose the electric field induced thermal Hall effect of triplons in the quantum dimer magnets  $X\text{CuCl}_3$  ( $X = \text{Tl}, \text{K}$ ), which exhibit spin-driven ferroelectricity in the Bose-Einstein condensation phase of triplons. The interplay between ferroelectricity and magnetism in these materials leads to the magnetoelectric effect, i.e., an electric-field induced Dzyaloshinskii-Moriya (DM) interaction between spins belonging to the same dimer. We argue that this intra-dimer DM interaction breaks the symmetry of the system in the absence of an electric field and gives rise to the thermal Hall effect, which can be detected in experimentally accessible electric and magnetic fields. We also show that the thermal Hall effect can be controlled by changing the strength or direction of the electric field.

*Introduction.*— Quantum spin systems exhibit a variety of interesting properties that are not present in their classical counterparts. Quantum dimer magnets are such examples, where the neighboring  $S = 1/2$  spins form dimers with a spin-singlet ( $S = 0$ ) ground state and triplet ( $S = 1$ ) bosonic excitations called triplons. The triplons undergo Bose-Einstein condensation (BEC) when the magnetic field exceeds a critical value [1–10]. In the BEC phase, the ground state of an individual dimer is a coherent superposition of the singlet and triplet states. This hybridization between the two states breaks the inversion symmetry and can lead to the spontaneous polarization on dimers. In particular,  $X\text{CuCl}_3$  ( $X = \text{Tl}, \text{K}$ ) is known to exhibit ferroelectricity in the BEC phase, whereas these materials have inversion centers at the center of dimers in the weak magnetic field regime [11–14]. When one applies an electric field in the BEC phase, the spin-dependent polarization can couple with the electric field, inducing the intra-dimer Dzyaloshinskii-Moriya (DM) interaction. It is thus natural to ask whether the transport of triplons in these materials can be significantly affected or controlled by the electric field.

Various transverse transport phenomena associated with the Berry curvature have been proposed for bosonic excitations such as magnons [15–45], photons [46–50], phonons [51–56], and triplons [57–63]. In particular, the thermal Hall effect of these charge-neutral bosons has attracted increasing attention in recent years as a powerful tool to gain information about the nature of elementary excitations. For example, the thermal Hall effect of magnons induced by the DM interactions has been observed [16, 18]. By contrast, the thermal Hall effect of triplons has yet to be detected experimentally [62], despite the theoretical prediction for the quantum dimer magnet  $\text{SrCu}_2(\text{BO}_3)_2$  [57].

In this Letter, we propose the electric field induced thermal Hall effect of triplons in the quantum dimer magnets  $X\text{CuCl}_3$  ( $X = \text{Tl}, \text{K}$ ). In addition to isotropic Heisenberg interactions considered in the previous studies [3–5], we take into account the symmetry-allowed

inter-dimer DM interactions as well as the electric field-induced intra-dimer DM interactions. In the absence of electric field, the system possesses an effective PT symmetry and does not exhibit the thermal Hall effect. However, the electric field-induced intra-dimer DM interactions break this symmetry, and thus lead to the thermal Hall effect. We also show that the magnitude (the direction) of the thermal Hall current can be controlled by manipulating the strength (the direction) of the electric field. The numerical results suggest that the thermal Hall effect in  $X\text{CuCl}_3$  can be observed in experimentally attainable electric and magnetic fields.

*The model.*—  $X\text{CuCl}_3$  is a three-dimensional interacting dimer system where the  $S = 1/2$  spins of  $\text{Cu}^{2+}$  ions form dimers due to the strong intra-dimer interactions [3–5] [see Fig. 1]. The unit cell contains two equivalent dimers, which belong to two different sublattices labeled as 1 and 2 in the following. The spin-1/2 operators  $\mathbf{S}_l^m(\mathbf{R})$  and  $\mathbf{S}_r^m(\mathbf{R})$  denote the left and right spins of the dimer in the unit cell at the position  $\mathbf{R}$  on the sublattice  $m (= 1, 2)$ , respectively. The lattice unit vectors  $\hat{a}$ ,  $\hat{b}$ , and  $\hat{c}$  correspond to the  $a$ ,  $b$ , and  $c$  axes in the materials, respectively. The Hamiltonian of the system is given by

$$\mathcal{H} = \mathcal{H}_{\text{Hei}} + \mathcal{H}_{\text{DM}} + \mathcal{H}_{\text{ext}}, \quad (1)$$

$$\mathcal{H}_{\text{Hei}} = \frac{1}{2} \sum_{\mathbf{R}, \mathbf{R}'} \sum_{\alpha, \beta} \sum_{m, n} J_{\alpha\beta}^{mn}(\mathbf{R}' - \mathbf{R}) \mathbf{S}_\alpha^m(\mathbf{R}) \cdot \mathbf{S}_\beta^n(\mathbf{R}'), \quad (2)$$

$$\mathcal{H}_{\text{DM}} = \frac{1}{2} \sum_{\mathbf{R}, \mathbf{R}'} \sum_{\alpha} \mathbf{D}_\alpha^{\text{int}}(\mathbf{R}' - \mathbf{R}) \cdot [\mathbf{S}_\alpha^1(\mathbf{R}) \times \mathbf{S}_\alpha^2(\mathbf{R}')], \quad (3)$$

$$\mathcal{H}_{\text{ext}} = - \sum_{\mathbf{R}} \sum_{\alpha=l,r} [g\mu_B \mathbf{H} \cdot \mathbf{S}_\alpha^m(\mathbf{R})] + \mathbf{E} \cdot \mathbf{P}^m(\mathbf{R}), \quad (4)$$

where the sums in Eqs. (2), (3), and (4) are taken over  $\alpha, \beta = l, r$  and the sublattice indices  $m, n = 1, 2$  ( $m \leq n$ ).

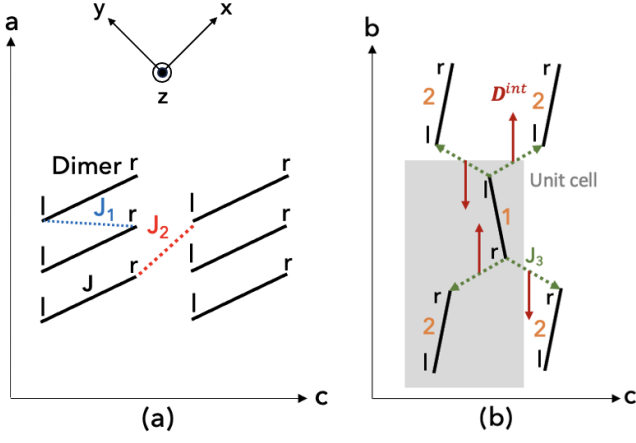


FIG. 1. A schematic picture of dimers and relevant interactions in  $XCuCl_3$ : (a)  $a$ - $c$  plane; (b)  $b$ - $c$  plane. The symbols  $l$  and  $r$  denote the left and right spins of each dimer. Thick black lines indicate the intra-dimer exchange coupling  $J$ , whereas the dotted blue, red, and green lines denote inter-dimer exchange couplings  $J_1$ ,  $J_2$ , and  $J_3$ , respectively. In (a),  $x$ ,  $y$ , and  $z$  axes are indicated. In (b), 1 and 2 are the sublattice indices, and the gray rectangle indicates the structural unit cell. The solid brown (dotted green) arrows represent the direction of (sign convention for)  $\mathbf{D}^{\text{int}}$ .

In the Hamiltonian  $\mathcal{H}_{\text{Hei}}$ ,  $J_{lr}^{mm}(\mathbf{0}) = J$  describes the antiferromagnetic intra-dimer exchange coupling, whereas  $J_{lr}^{mm}(\hat{a}) = J_1$  and  $J_{lr}^{mm}(2\hat{a} + \hat{c}) = J_2$  are exchange couplings between the spins belonging to the same sublattices [see Fig. 1 (a)]. The model also includes Heisenberg interactions between the spins on the different sublattices:  $J_{rr}^{12}(\mathbf{0}) = J_{rr}^{12}(2\hat{a} + \hat{c}) = J_{ll}^{12}(\hat{b}) = J_{ll}^{12}(2\hat{a} + \hat{b} + \hat{c}) = J_3$  [see Fig. 1 (b)]. The Hamiltonian  $\mathcal{H}_{\text{Hei}}$  has been studied as a minimal model of  $XCuCl_3$  [3–5]. The Hamiltonian  $\mathcal{H}_{\text{DM}}$  in Eq. (3) describes the symmetry-allowed inter-dimer DM interactions, where  $\mathbf{D}_r^{\text{int}}(\mathbf{0}) = \mathbf{D}_l^{\text{int}}(2\hat{a} + \hat{b} + \hat{c}) = D^{\text{int}}\hat{b}$  and  $\mathbf{D}_r^{\text{int}}(2\hat{a} + \hat{c}) = \mathbf{D}_l^{\text{int}}(\hat{b}) = -D^{\text{int}}\hat{b}$  are inter-dimer DM vectors parallel to the  $b$  axis [see Fig. 1 (b)]. See Supplemental Material for details of the derivation of the relative signs of these DM vectors [64]. Here, we do not consider the other components of the inter-dimer DM vectors allowed by crystal symmetry since their contribution to the thermal Hall effect is negligible. The remaining interactions in Eqs. (2) and (3) are zero. The experimental values of the above mentioned parameters are listed in Table I. Equation (4) describes the Zeeman term and the polarization term of  $XCuCl_3$ , where  $g = 2.06$  for  $\mathbf{H} \parallel b$  [6] is the g-factor,  $\mu_B$  is the Bohr magneton,  $\mathbf{H}$  is the magnetic field parallel to the  $b$  axis,  $\mathbf{E}$  is the electric field, and  $\mathbf{P}^m(\mathbf{R})$  is the local polarization on each dimer. To simplify the analysis, we use the coordinate system as  $x \parallel \hat{a} + \hat{c}/2$ ,  $y \parallel \hat{a} - \hat{c}/2$ ,  $z \parallel \hat{b}$  where  $\hat{a} \perp \hat{b} \perp \hat{c}$ ,  $2a \sim c$ , and  $2\sqrt{2}a \sim b$  hold approximately for these materials [2] [see Fig. 1 (a)].

The polarization term in Eq. (4) can be interpreted

as the electric field-induced intra-dimer DM interaction term

$$-\mathbf{E} \cdot \mathbf{P}^m(\mathbf{R}) = \mathbf{D}^{\text{ext},m} \cdot [\mathbf{S}_l^m(\mathbf{R}) \times \mathbf{S}_r^m(\mathbf{R})]. \quad (5)$$

Here the intra-dimer DM vector  $\mathbf{D}^{\text{ext},m}$  can be written in terms of the polarization tensor of each sublattice  $\tilde{C}^m$  that has nine independent components  $C_{\mu\nu}^m$  ( $\mu, \nu = x, y, z$ ) [12–14, 65]

$$D_{\nu}^{\text{ext},m} = -E_{\mu'} C_{\mu'\nu}^m, \quad (6)$$

where repeated indices are summed over. In the above expression,  $D_{\nu}^{\text{ext},m}$  and  $E_{\nu}$  ( $\nu = x, y, z$ ) are the  $\nu$ -component of  $\mathbf{D}^{\text{ext},m}$  and  $\mathbf{E}$ . The two tensors  $C_{\mu\nu}^1$  and  $C_{\mu\nu}^2$  are related by

$$C_{\mu\nu}^2 = -\gamma_{\mu\mu'} C_{\mu'\nu'}^1 \gamma_{\nu\nu'}, \quad (7)$$

where  $\gamma = \text{diag}(1, 1, -1)$ . See Supplemental Material for details of the derivation of Eqs. (6) and (7) [64]. The experimental values of  $C_{\mu\nu}^1$  obtained in the previous studies [14] are listed in Table II. We ignore the  $z$  component of the electric field-induced intra-dimer DM interaction term in the later analysis [66].

Parameter	$J$	$J_1$	$J_2$	$J_3$	$D^{\text{int}}$
Energy	5.5	0.43	3.16	0.91	–

TABLE I. Experimental values of the interactions (in meV) for  $X = \text{Tl}$  [5]. The value of  $D^{\text{int}}$  is undetermined in the previous studies [3–5].

$C_{\mu\nu}^1$	$C_{xx}^1$	$C_{xy}^1$	$C_{yx}^1$	$C_{yy}^1$	$C_{zx}^1$	$C_{zy}^1$	$C_{zz}^1$
Values	–27.5	–5	–32.5	124.5	–	–	2.5

TABLE II. Experimental values of the polarization tensor  $C_{\mu\nu}^1$  (in  $\mu\text{C}/\text{m}^2$ ) for  $X = \text{Tl}$  [67]. The values of  $C_{zx}^1$ , and  $C_{zy}^1$  are undetermined in the previous studies [11, 12, 14]. The values of  $C_{xz}^1$  and  $C_{yz}^1$  are not used in our study.

*Methods.*— In order to investigate the excitation spectrum and the transport properties of the systems, we introduce bond operators  $s_{\mathbf{R}\alpha}^{m\dagger}$  and  $t_{\mathbf{R}\alpha}^{m\dagger}$  ( $\alpha = +, 0, -$ ) that create the singlet state  $|s\rangle_{\mathbf{R}}^m$  and the three triplet states  $|t_{\alpha}\rangle_{\mathbf{R}}^m$  out of the vacuum  $|0\rangle_{\mathbf{R}}^m$  on each dimer [3–5, 68]:

$$\begin{aligned} |s\rangle_{\mathbf{R}}^m &= s_{\mathbf{R}}^{m\dagger} |0\rangle_{\mathbf{R}}^m = \frac{1}{\sqrt{2}}(|\uparrow\downarrow\rangle_{\mathbf{R}}^m - |\downarrow\uparrow\rangle_{\mathbf{R}}^m), \\ |t_{+}\rangle_{\mathbf{R}}^m &= t_{\mathbf{R}+}^{m\dagger} |0\rangle_{\mathbf{R}}^m = -|\uparrow\uparrow\rangle_{\mathbf{R}}^m, \\ |t_{0}\rangle_{\mathbf{R}}^m &= t_{\mathbf{R}0}^{m\dagger} |0\rangle_{\mathbf{R}}^m = \frac{1}{\sqrt{2}}(|\uparrow\downarrow\rangle_{\mathbf{R}}^m + |\downarrow\uparrow\rangle_{\mathbf{R}}^m), \\ |t_{-}\rangle_{\mathbf{R}}^m &= t_{\mathbf{R}-}^{m\dagger} |0\rangle_{\mathbf{R}}^m = |\downarrow\downarrow\rangle_{\mathbf{R}}^m, \end{aligned} \quad (8)$$

where  $\mathbf{R}$  and  $m$  denote the position of the unit cell and the sublattice index. These obey Bose statistics and are

subject to the constraint  $s_{\mathbf{R}}^{m\dagger} s_{\mathbf{R}}^m + \sum_{\alpha=+,0,-} t_{\mathbf{R}\alpha}^{m\dagger} t_{\mathbf{R}\alpha}^m = 1$  on each dimer. In the BEC phase, the ground state is well represented by a coherent superposition of the singlet and triplet states on each dimer [5, 11]

$$|\text{GS}\rangle_{\mathbf{R}}^m = \cos\theta_m |s\rangle_{\mathbf{R}}^m + \sin\theta_m \exp(i\phi_m) |t_+\rangle_{\mathbf{R}}^m, \quad (9)$$

where  $\theta_m$  and  $\phi_m$  are variational parameters for each sublattice  $m$ . In Eq. (9) and the following analysis, we focus on the high magnetic field regimes  $H \geq 40$  T for  $X = \text{Tl}$  and  $H \geq 25$  T for  $X = \text{K}$  in  $X\text{CuCl}_3$ , where the contribution of the other two triplet modes to the ground state (9) can be neglected [5].

To analyze the excited states, we perform the following unitary transformation

$$\begin{aligned} a_{\mathbf{R}}^{m\dagger} &= \cos\theta_m s_{\mathbf{R}}^{m\dagger} + \sin\theta_m \exp(i\phi_m) t_{\mathbf{R}+}^{m\dagger}, \\ b_{\mathbf{R}+}^{m\dagger} &= -\sin\theta_m s_{\mathbf{R}}^{m\dagger} + \cos\theta_m \exp(i\phi_m) t_{\mathbf{R}+}^{m\dagger}, \\ b_{\mathbf{R}0}^{m\dagger} &= t_{\mathbf{R}0}^{m\dagger}, \\ b_{\mathbf{R}-}^{m\dagger} &= t_{\mathbf{R}-}^{m\dagger}, \end{aligned} \quad (10)$$

which preserves the particle number constraint, i.e.,  $a_{\mathbf{R}}^{m\dagger} a_{\mathbf{R}}^m + \sum_{\alpha=+,0,-} b_{\mathbf{R}\alpha}^{m\dagger} b_{\mathbf{R}\alpha}^m = 1$ . We follow the standard procedure and replace  $a_{\mathbf{R}}^{m\dagger} a_{\mathbf{R}}^m$  with  $1 - 1/N \sum_{\mathbf{R},\alpha} b_{\mathbf{R},\alpha}^{m\dagger} b_{\mathbf{R},\alpha}^m$  where  $N$  is the number of dimers on the sublattice  $m$ . This assumption is justified at low temperatures. By introducing the Fourier transform:  $b_{\mathbf{R}\alpha}^{m\dagger} = 1/N \sum_{\mathbf{k}\alpha} b_{\mathbf{k}\alpha}^{m\dagger} e^{i\mathbf{k}\cdot\mathbf{R}^m}$  ( $\mathbf{R}^1 = \mathbf{R}$ , and  $\mathbf{R}^2 = \mathbf{R} - (\hat{a} + \hat{b}/2 + \hat{c}/2)$ ) and retaining only up to quadratic order in  $b_{\mathbf{k}\alpha}^{m\dagger}$  and  $b_{\mathbf{k}\alpha}^m$ , the Hamiltonian (1) takes the form  $\mathcal{H} = \mathcal{H}^{(0)} + \mathcal{H}^{(1)} + \mathcal{H}^{(2)}$ . Here the constant term  $\mathcal{H}^{(0)}$  represents the energy of the variational ground state and  $\mathcal{H}^{(1)}$  ( $\mathcal{H}^{(2)}$ ) is the linear (quadratic) term in bosonic operators. The linear term  $\mathcal{H}^{(1)}$  vanishes when we choose the parameters  $\theta_m$ ,  $\phi_m$  to minimize  $\mathcal{H}^{(0)}$ . Details of the explicit expression of  $\mathcal{H}^{(0)}$  term and the variational equations are given in Supplemental Material [64]. The quadratic term  $\mathcal{H}^{(2)}$  represents the bosonic Bogoliubov-de Gennes (BdG) Hamiltonian described in the  $12 \times 12$  matrix form.

*Low-energy effective model.*— Here, we construct the low-energy effective model for ease of analysis. When the magnetic field is strong, the energy of the lowest excitation mode and those of the other two modes are sufficiently separated [5]. For this reason, we consider only the operators  $b_+^\dagger$  and  $b_+$  to discuss the thermal Hall effect in the high magnetic field and low-temperature regimes. As a result, we obtain the BdG Hamiltonian described in the  $4 \times 4$  matrix form with a vector  $\mathbf{b}_{\mathbf{k}} = (b_{\mathbf{k}+}^1, b_{\mathbf{k}+}^2, b_{-\mathbf{k}+}^1, b_{-\mathbf{k}+}^2)^T$  as

$$\mathcal{H}^{(2)} \simeq \frac{1}{2} \sum_{\mathbf{k}} \mathbf{b}_{\mathbf{k}}^\dagger H_{\text{BdG}}(\mathbf{k}) \mathbf{b}_{\mathbf{k}}, \quad (11)$$

$$H_{\text{BdG}}(\mathbf{k}) = \begin{pmatrix} \Xi(\mathbf{k}) & \Pi(\mathbf{k}) \\ \Pi^*(-\mathbf{k}) & \Xi^*(-\mathbf{k}) \end{pmatrix}. \quad (12)$$

The explicit expression of the matrix (12) is given in Supplemental Material [64].

To preserve the bosonic commutation relations, the BdG Hamiltonian (12) has to be diagonalized using a paraunitary matrix  $T(\mathbf{k})$ . The matrix satisfies  $T^\dagger(\mathbf{k}) \Sigma_z T(\mathbf{k}) = \Sigma_z$ , where  $\Sigma_z = \text{diag}(1, 1, -1, -1)$ . The BdG Hamiltonian is diagonalized as

$$\Sigma_z H_{\text{BdG}}(\mathbf{k}) T(\mathbf{k}) = T(\mathbf{k}) \Sigma_z E(\mathbf{k}), \quad (13)$$

where the diagonal matrix  $E(\mathbf{k})$  takes the form  $E(\mathbf{k}) = \text{diag}(E_1(\mathbf{k}), E_2(\mathbf{k}), E_1(-\mathbf{k}), E_2(-\mathbf{k}))$ . The positive energies  $E_1(\mathbf{k})$  and  $E_2(\mathbf{k})$  correspond to the upper and lower particle bands, respectively. In order to calculate the thermal Hall conductivity, it is sufficient to consider these two bands [19, 21].

*Thermal Hall effect.*— We here provide the expression of the three-dimensional thermal Hall effect in the  $z$ - $x$  plane. The thermal Hall conductivity of the bosonic BdG system is given by [21]

$$\kappa_{zx} = -\frac{k_B^2 T}{\hbar} \sum_{n=1}^2 \int_{\text{BZ}} \frac{d^3 k}{(2\pi)^3} \left[ c_2(\rho(E_n(\mathbf{k}))) - \frac{\pi^2}{3} \right] \Omega_n^y(\mathbf{k}), \quad (14)$$

where  $k_B$  is the Boltzmann constant,  $T$  is the temperature of the system,  $\hbar$  is the Planck constant, and  $\rho(E_n(\mathbf{k})) = 1/(e^{\beta E_n(\mathbf{k})} - 1)$  is the Bose distribution function with  $\beta$  being the inverse temperature. The explicit form of  $c_2(\rho)$  is given by

$$\begin{aligned} c_2(\rho) &= \int_0^\rho dt \left( \log \frac{1+t}{t} \right)^2 \\ &= (1+\rho) \left( \log \frac{1+\rho}{\rho} \right)^2 - (\log \rho)^2 - 2\text{Li}_2(-\rho), \end{aligned} \quad (15)$$

where  $\text{Li}_2(x)$  is the dilogarithm function. The Berry curvature of the  $n$ th band  $\Omega_n^y(\mathbf{k})$  is defined as

$$\Omega_n^y(\mathbf{k}) = -2\text{Im} \left[ \Sigma_z \frac{\partial T^\dagger(\mathbf{k})}{\partial k_z} \Sigma_z \frac{\partial T(\mathbf{k})}{\partial k_x} \right]_{nn}. \quad (16)$$

*Results.*— Figure 2 shows the numerical results of the thermal Hall conductivity  $\kappa_{zx}$  in Eq. (14). In the numerical calculation [69], we set the moderate values of  $|\mathbf{D}^{\text{int}}|$ ,  $C_{zx}^1$ , and  $C_{zy}^1$  (see the caption of Fig. 2) that are undetermined in the previous studies [3-5, 11, 12, 14].

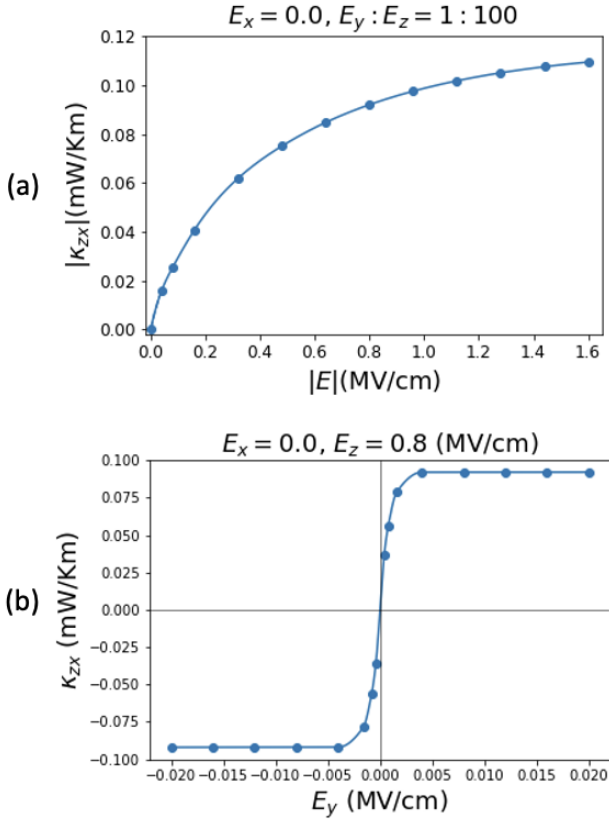


FIG. 2. (a) The absolute value of the thermal Hall conductivity  $|\kappa_{zx}|$  as a function of the strength of the electric field with  $E_x = 0.0$  MV/cm and  $E_y : E_z = 1 : 100$ . (b) The thermal Hall conductivity  $\kappa_{zx}$  as a function of  $E_y$  with  $E_x = 0.0$  MV/cm and  $E_z = 0.8$  MV/cm. The parameters used for (a), and (b) are listed in Table I and II. We set the moderate values for the undetermined parameters as  $D^{\text{int}} = 0.091$  meV,  $C_{zx}^1 = -16.3 \mu\text{C}/\text{m}^2$ , and  $C_{zy}^1 = 62.3 \mu\text{C}/\text{m}^2$ . The magnetic field and temperature are  $H = 42$  T and  $T = 10$  K, respectively.

From Fig. 2 (a), we find that increasing the strength of the electric field leads to the enhancement of  $|\kappa_{zx}|$ . This behavior is consistent with the approximate expression of  $|\kappa_{zx}|$  in the high-temperature limit. Details of the discussion are given in the next section. The obtained values in Fig. 2 (a) are comparable to the experimental values of the thermal Hall conductivity of magnons and phonons [16, 18, 35, 45, 51] and thus are expected to be experimentally accessible. In addition, the applied electric field whose strength is of the order of 0.1 MV/cm is realizable in experiments [70].

Fig. 2 (b) indicates that the sign reversal of  $E_y$  results in the sign reversal of  $\kappa_{zx}$ . This result suggests that the direction of the Hall current can be controlled by changing the direction of the electric field in the  $x$ - $y$  plane. This can be understood as follows. The sign reversal of  $E_x$  and  $E_y$  leads to the exchange between  $\mathbf{D}^{\text{ext},1} \leftrightarrow \mathbf{D}^{\text{ext},2}$ , and thus the ground state wave functions of sublattice 1 and 2 [see Eq. (9)] are also swapped. Consequently, when we take complex conjugation of the BdG Hamiltonian (12)

with the inverse signs of  $E_x$  and  $E_y$  and changing the sublattice index as  $1 \leftrightarrow 2$ , the BdG Hamiltonian almost returns to the original one [71]. This implies that the sign change of  $E_x$  and  $E_y$  corresponds to the approximate time reversal operation, which leads to the reversal of the Hall current as shown in Fig. 2 (b). The constant like behavior for  $|E_y| \geq 0.004$  MV/cm reflects the fact that the ground state (9) does not change much by varying  $|E_y|$  due to  $|C_{zy}^1 E_z| \gg |C_{yy}^1 E_y|$  [72]

We expect the same behavior for  $X = \text{K}$  as for  $X = \text{Tl}$  in  $\text{XCuCl}_3$  in the above results. However, it is more difficult to obtain reliable results in the  $X = \text{K}$  case since there are more undetermined parameters than in the  $X = \text{Tl}$  case.

*Discussion.*— Here, we explain how the electric field induces and enhances the thermal Hall effect as in Fig. 2 (a). In the absence of an electric field, the difference between the variational parameters  $\theta_1 - \theta_2$  and  $\phi_1 - \phi_2$  in Eq. (9) are 0 and  $\pm\pi$ , respectively [3–5]. In this case, the Berry curvature is absent due to the effective PT symmetry of the BdG Hamiltonian (12). However, the applied electric field gives rise to the difference between  $\theta_1$  and  $\theta_2$ , which breaks the above symmetry, resulting in the nonzero thermal Hall effect. See Supplemental Material for details [64].

We now argue that the electric field can open and control the band gap. Before applying the electric field, there are gapless lines  $G_{\pm,j}$  in the Brillouin zone:  $G_{+,j} = (j\pi, k_y, \frac{\pi}{2})$ ,  $G_{-,j} = (\frac{2j-1}{2}\pi, k_y, 0)$  ( $j = 0, 1$ ). However, the applied electric field opens the band gap at  $G_{\pm,j}$ , each of which is a source of the Berry curvature as shown in Fig. (3).

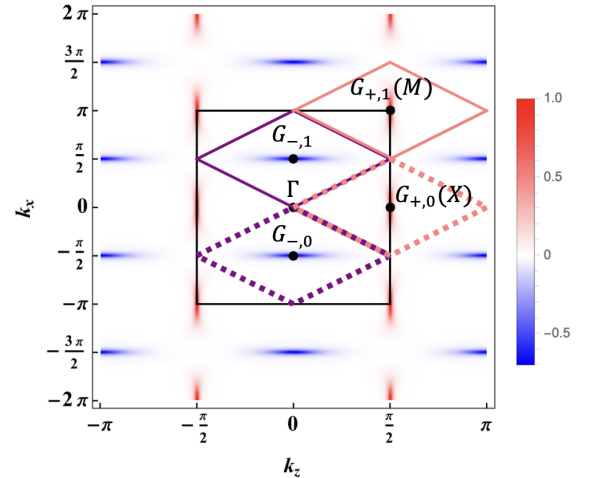


FIG. 3. Distribution of the Berry curvature of the upper band ( $n = 1$ ) in the  $k_z$ - $k_x$  plane with  $k_y = 0$  under the applied electric field  $\mathbf{E} = (0.0, 0.016, 1.6)$  MV/cm. The area enclosed by the black square denotes the first Brillouin zone (BZ). The areas enclosed by the pink and purple rhombuses indicate the region  $S_{+,j}(0)$  and  $S_{-,j}(0)$ , respectively (the solid ones for  $j = 1$ , and the dashed ones for  $j = 0$ ). The Berry curvature is normalized in this figure so that the maximum value is 1.

For a fixed direction of the electric field, the band gap at  $G_{\pm,j}$ , which we denote by  $E_{\text{gap},\pm,j}(k_y)$ , behaves as

$$E_{\text{gap},\pm,j}(k_y) \propto |\mathbf{E}|. \quad (17)$$

See Supplemental Material for derivation [64]. Let us show that the electric field can increase the thermal Hall conductivity  $\kappa_{zx}$  by widening the band gap at  $G_{\pm,j}$ . For a rough estimation, we consider the high-temperature asymptotic form of  $\kappa_{zx}$  in the following. In the temperature region  $k_B T \gg E_1(j\pi, k_y, \frac{\pi}{2}), E_1(\frac{2j-1}{2}\pi, k_y, 0)$ , we can apply the asymptotic form of  $c_2(\rho) \sim \frac{\pi^2}{3} - \frac{1}{\rho}$  ( $\rho \rightarrow \infty$ ) [73]. By assuming that the Berry curvature is localized at  $G_{\pm,j}$  and using  $e^{\beta E_n(\mathbf{k})} \simeq 1 + \beta E_n(\mathbf{k})$ ,  $\Omega_1^y(\mathbf{k}) = -\Omega_2^y(\mathbf{k})$ , and Eq. (17), we have

$$\begin{aligned} |\kappa_{zx}| &\simeq \frac{k_B^2 T}{\hbar} \left| \int_{\text{BZ}} \frac{d^3 k}{(2\pi)^3} \left[ \frac{E_1(\mathbf{k}) - E_2(\mathbf{k})}{k_B T} \right] \Omega_1^y(\mathbf{k}) \right| \\ &\simeq \frac{k_B}{8\pi^3 \hbar} \left| \sum_{\sigma,j} \int_{k_y} dk_y E_{\text{gap},\sigma,j}(k_y) \int_{S_{\sigma,j}(k_y)} dk_z dk_x \Omega_1^y(\mathbf{k}) \right| \\ &\simeq \frac{k_B}{8\pi^2 \hbar} |E_{\text{gap},+} - E_{\text{gap},-}| \propto |\mathbf{E}|, \end{aligned} \quad (18)$$

where the region  $S_{\pm,j}(k_y)$  is the area enclosed by the rhombus around  $G_{\pm,j}$  in Fig. (3), and we have defined the average band gaps as  $E_{\text{gap},\pm} = \frac{1}{2} \sum_j \int_{k_y} dk_y E_{\text{gap},\pm,j}(k_y)$ . In going from the second to the third line, we used  $|\int_{S_{\pm,j}(k_y)} dk_z dk_x \Omega_1^y(\mathbf{k})| \simeq \frac{\pi}{2}$ . Clearly, Eq. (18) shows that  $|\kappa_{zx}|$  increases with increasing electric field.

Under the applied magnetic field  $H = 42$  T and the electric field  $\mathbf{E} = (0, 0.016, 1.6)$  MV/cm, the values of the average band gaps are  $E_{\text{gap},+} \simeq 0.059$  meV/Å and  $E_{\text{gap},-} \simeq 0.041$  meV/Å. Hence, the absolute value of the thermal Hall conductivity in the high-temperature limit (18) is estimated as 0.048 mW/Km, whose order of magnitude is consistent with the numerical result in Fig. 2 (a).

*Conclusion and outlook.*— In this Letter, we have proposed the electric field induced thermal Hall effect of triplons in the quantum dimer magnets  $XCuCl_3$  ( $X = \text{Tl}, \text{K}$ ). We analyzed the isotropic Heisenberg model

with symmetry-allowed inter-dimer and the electric field-induced intra-dimer DM interactions. In this model, the low-energy behavior can be well described by the lowest triplon mode in the high magnetic field regimes, i.e.,  $H \geq 40$  T for  $X = \text{Tl}$  and  $H \geq 25$  T for  $X = \text{K}$ . We showed that the electric field breaks the effective PT symmetry of the Hamiltonian and thus induces the thermal Hall effect. Furthermore, the electric field widens the band gap, leading to the enhancement of the thermal Hall effect. We also showed that the sign change of  $E_x$  and  $E_y$  corresponds to the approximate time reversal operation, which reverses the direction of the Hall current. We expect that these behaviors can be observed experimentally in realistic electric and magnetic fields.

Here, we note that even in the lower magnetic field regime, we expect the nonzero thermal Hall effect in  $XCuCl_3$  and its electric field control. However, the analysis is more complicated since the other triplet modes are relevant in this regime. The detailed analysis is left for future work.

The theory presented here can be applied to other quantum dimer magnets with ferroelectricity or paraelectricity. Moreover, if the pressure induces the intra-dimer DM interaction [74, 75], it can play the same role as the electric field in the present model. Finally, our theory suggests that the measurement of the thermal Hall conductivity provides constraints on the unknown elements of the polarization tensor  $C_{zx}^1$  and  $C_{zy}^1$  in  $XCuCl_3$  ( $X = \text{Tl}, \text{K}$ ), which will be useful for future studies.

## ACKNOWLEDGMENTS

We thank Kosuke Fujiwara, Shojiro Kimura, and Karlo Penc for useful discussions. This work was supported by JSPS KAKENHI Grants No. JP18K03445, No. JP20K14411, MEXT KAKENHI Grant-in-Aid for Scientific Research on Innovative Areas ‘‘Quantum Liquid Crystals’’ (KAKENHI Grant No. JP22H04469), and for Transformative Research Areas A ‘‘Extreme Universe’’ (KAKENHI Grant No. JP21H05191). N.E. was supported by Forefront Physics and Mathematics Program to Drive Transformation (FoPM), a World-leading Innovative Graduate Study (WINGS) Program, the University of Tokyo. Y.A. was supported by JST PRESTO Grant No. JPMJPR2251.

\* esaki-nanse0428@g.ecc.u-tokyo.ac.jp

- [1] T. Nikuni, M. Oshikawa, A. Oosawa, and H. Tanaka, Phys. Rev. Lett. **84**, 5868 (2000).  
 [2] H. Tanaka, A. Oosawa, T. Kato, H. Uekusa, Y. Ohashi, K. Kakurai, and A. Hoser, J. Phys. Soc. Jpn. **70**, 939 (2001).  
 [3] M. Matsumoto, B. Normand, T. Rice, and M. Sigrist,

Phys. Rev. Lett. **89**, 077203 (2002).

- [4] A. Oosawa, T. Takamasu, K. Tatani, H. Abe, N. Tsujii, O. Suzuki, H. Tanaka, G. Kido, and K. Kindo, Phys. Rev. B **66**, 104405 (2002).  
 [5] M. Matsumoto, B. Normand, T. a. Rice, and M. Sigrist, Phys. Rev. B **69**, 054423 (2004).  
 [6] F. Yamada, T. Ono, H. Tanaka, G. Misguich, M. Os-

- hikawa, and T. Sakakibara, *J. Phys. Soc. Jpn.* **77**, 013701 (2007).
- [7] T. Giamarchi, C. Rüegg, and O. Tchernyshyov, *Nat. Phys.* **4**, 198 (2008).
- [8] N. Cavadini, G. Heigold, W. Henggeler, A. Furrer, H.-U. Güdel, K. Krämer, and H. Mutka, *Phys. Rev. B* **63**, 172414 (2001).
- [9] N. Cavadini, C. Rüegg, A. Furrer, H.-U. Güdel, K. Krämer, H. Mutka, and P. Vorderwisch, *Phys. Rev. B* **65**, 132415 (2002).
- [10] C. Rüegg, N. Cavadini, A. Furrer, H.-U. Güdel, K. Krämer, H. Mutka, A. Wildes, K. Habicht, and P. Vorderwisch, *Nature* **423**, 62 (2003).
- [11] S. Kimura, K. Kakihata, Y. Sawada, K. Watanabe, M. Matsumoto, M. Hagiwara, and H. Tanaka, *Nat. Commun.* **7**, 12822 (2016).
- [12] S. Kimura, K. Kakihata, Y. Sawada, K. Watanabe, M. Matsumoto, M. Hagiwara, and H. Tanaka, *Phys. Rev. B* **95**, 184420 (2017).
- [13] S. Kimura, M. Matsumoto, M. Akaki, M. Hagiwara, K. Kindo, and H. Tanaka, *Phys. Rev. B* **97**, 140406 (2018).
- [14] S. Kimura, M. Matsumoto, and H. Tanaka, *Phys. Rev. Lett.* **124**, 217401 (2020).
- [15] H. Katsura, N. Nagaosa, and P. A. Lee, *Phys. Rev. Lett.* **104**, 066403 (2010).
- [16] Y. Onose, T. Ideue, H. Katsura, Y. Shiomi, N. Nagaosa, and Y. Tokura, *Science* **329**, 297 (2010).
- [17] R. Matsumoto and S. Murakami, *Phys. Rev. Lett.* **106**, 197202 (2011).
- [18] T. Ideue, Y. Onose, H. Katsura, Y. Shiomi, S. Ishiwata, N. Nagaosa, and Y. Tokura, *Phys. Rev. B* **85**, 134411 (2012).
- [19] R. Shindou, R. Matsumoto, S. Murakami, and J.-i. Ohe, *Phys. Rev. B* **87**, 174427 (2013).
- [20] L. Zhang, J. Ren, J.-S. Wang, and B. Li, *Phys. Rev. B* **87**, 144101 (2013).
- [21] R. Matsumoto, R. Shindou, and S. Murakami, *Phys. Rev. B* **89**, 054420 (2014).
- [22] A. Mook, J. Henk, and I. Mertig, *Phys. Rev. B* **89**, 134409 (2014).
- [23] B. Xu, T. Ohtsuki, and R. Shindou, *Phys. Rev. B* **94**, 220403 (2016).
- [24] A. Mook, J. Henk, and I. Mertig, *Phys. Rev. B* **99**, 014427 (2019).
- [25] H. Kondo, Y. Akagi, and H. Katsura, *Phys. Rev. B* **99**, 041110 (2019).
- [26] M. Kawano and C. Hotta, *Phys. Rev. B* **99**, 054422 (2019).
- [27] H. Kondo, Y. Akagi, and H. Katsura, *Phys. Rev. B* **100**, 144401 (2019).
- [28] S. K. Kim, K. Nakata, D. Loss, and Y. Tserkovnyak, *Phys. Rev. Lett.* **122**, 057204 (2019).
- [29] Y. Akagi, *J. Phys. Soc. Jpn.* **89**, 123601 (2020).
- [30] H. Kondo, Y. Akagi, and H. Katsura, *Progress of Theoretical and Experimental Physics* **2020**, 12A104 (2020).
- [31] H. Kondo and Y. Akagi, *Phys. Rev. Lett.* **127**, 177201 (2021).
- [32] H. Kondo and Y. Akagi, *Phys. Rev. Res.* **4**, 013186 (2022).
- [33] K. Fujiwara, S. Kitamura, and T. Morimoto, *Phys. Rev. B* **106**, 035113 (2022).
- [34] R. R. Neumann, A. Mook, J. Henk, and I. Mertig, *Phys. Rev. Lett.* **128**, 117201 (2022).
- [35] M. Hirschberger, R. Chisnell, Y. S. Lee, and N. P. Ong, *Phys. Rev. Lett.* **115**, 106603 (2015).
- [36] R. Chisnell, J. Helton, D. Freedman, D. Singh, R. Bewley, D. Nocera, and Y. Lee, *Phys. Rev. Lett.* **115**, 147201 (2015).
- [37] P. McClarty, X.-Y. Dong, M. Gohlke, J. Rau, F. Pollmann, R. Moessner, and K. Penc, *Phys. Rev. B* **98**, 060404 (2018).
- [38] T. Cookmeyer and J. E. Moore, *Phys. Rev. B* **98**, 060412 (2018).
- [39] D. G. Joshi, *Phys. Rev. B* **98**, 060405 (2018).
- [40] Y. Shiomi, R. Takashima, and E. Saitoh, *Phys. Rev. B* **96**, 134425 (2017).
- [41] R. Cheng, S. Okamoto, and D. Xiao, *Phys. Rev. Lett.* **117**, 217202 (2016).
- [42] V. A. Zyuzin and A. A. Kovalev, *Phys. Rev. Lett.* **117**, 217203 (2016).
- [43] K. Hwang, N. Trivedi, and M. Randeria, *Phys. Rev. Lett.* **125**, 047203 (2020).
- [44] P. Laurell and G. A. Fiete, *Phys. Rev. Lett.* **118**, 177201 (2017).
- [45] H. Doki, M. Akazawa, H.-Y. Lee, J. H. Han, K. Sugii, M. Shimozawa, N. Kawashima, M. Oda, H. Yoshida, and M. Yamashita, *Phys. Rev. Lett.* **121**, 097203 (2018).
- [46] S. Raghu and F. D. M. Haldane, *Phys. Rev. A* **78**, 033834 (2008).
- [47] A. Petrescu, A. A. Houck, and K. Le Hur, *Phys. Rev. A* **86**, 053804 (2012).
- [48] M. C. Rechtsman, J. M. Zeuner, Y. Plotnik, Y. Lumer, D. Podolsky, F. Dreisow, S. Nolte, M. Segev, and A. Szameit, *Nature* **496**, 196 (2013).
- [49] M. Hafezi, S. Mittal, J. Fan, A. Migdall, and J. Taylor, *Nat. Photonics* **7**, 1001 (2013).
- [50] P. Ben-Abdallah, *Phys. Rev. Lett.* **116**, 084301 (2016).
- [51] C. Strohm, G. Rikken, and P. Wyder, *Phys. Rev. Lett.* **95**, 155901 (2005).
- [52] L. Sheng, D. Sheng, and C. Ting, *Phys. Rev. Lett.* **96**, 155901 (2006).
- [53] Y. Kagan and L. Maksimov, *Phys. Rev. Lett.* **100**, 145902 (2008).
- [54] L. Zhang, J. Ren, J.-S. Wang, and B. Li, *Phys. Rev. Lett.* **105**, 225901 (2010).
- [55] L. Zhang, J. Ren, J.-S. Wang, and B. Li, *J. Phys. Condens.* **23**, 305402 (2011).
- [56] T. Qin, J. Zhou, and J. Shi, *Phys. Rev. B* **86**, 104305 (2012).
- [57] J. Romhányi, K. Penc, and R. Ganesh, *Nat. Commun.* **6**, 6805 (2015).
- [58] M. Malki and K. Schmidt, *Phys. Rev. B* **95**, 195137 (2017).
- [59] P. A. McClarty, F. Krüger, T. Guidi, S. Parker, K. Refson, A. Parker, D. Prabhakaran, and R. Coldea, *Nat. Phys.* **13**, 736 (2017).
- [60] H. Sun, P. Sengupta, D. Nam, and B. Yang, *Phys. Rev. B* **103**, L140404 (2021).
- [61] D. Bhowmick and P. Sengupta, *Phys. Rev. B* **104**, 085121 (2021).
- [62] S. Suetsugu, T. Yokoi, K. Totsuka, T. Ono, I. Tanaka, S. Kasahara, Y. Kasahara, Z. Chengchao, H. Kageyama, and Y. Matsuda, *Phys. Rev. B* **105**, 024415 (2022).
- [63] A. Thomasen, K. Penc, N. Shannon, and J. Romhányi, *Phys. Rev. B* **104**, 104412 (2021).
- [64] See Supplemental Material for details.
- [65] T. A. Kaplan and S. D. Mahanti, *Phys. Rev. B* **83**, 174432

- (2011).
- [66] In the later analysis, we only focus on the lowest triplon mode. Since the  $z$ -component of the electric field-induced intra-dimer DM interaction term barely affects the lowest mode, we can ignore the  $z$  component in the present analysis.
- [67] The values in Table II are taken from [14]. Although the values in Table II look different from the values in [14], they are consistent if we use the same coordinate system as in [14].
- [68] S. Sachdev and R. Bhatt, Phys. Rev. B **41**, 9323 (1990).
- [69] We used the method in Ref. [76].
- [70] T. Lottermoser, T. Lonkai, U. Amann, D. Hohlwein, J. Ihringer, and M. Fiebig, Nature **430**, 541 (2004).
- [71] Usually, the BdG Hamiltonian does not exactly return to the original one due to  $\phi_2 - \phi_1 \neq \pm\pi$ . However, the difference from  $\pm\pi$  is small enough to be neglected.
- [72] The ground state (9) drastically changes around  $|E_y| = 0$ , where  $\kappa_{zx}$  shows a sharp change.
- [73] R. Samajdar, S. Chatterjee, S. Sachdev, and M. S. Scheurer, Phys. Rev. B **99**, 165126 (2019).
- [74] O. M. Volkov, D. D. Sheka, Y. Gaididei, V. P. Kravchuk, U. K. Rößler, J. Fassbender, and D. Makarov, Sci. Rep. **8**, 866 (2018).
- [75] Y. Xing, H. Chen, N. Xu, X. Li, and L. Zhang, Phys. Rev. B **105**, 104409 (2022).
- [76] T. Fukui, Y. Hatsugai, and H. Suzuki, J. Phys. Soc. Jpn. **74**, 1674 (2005).
- [77] We can usually ignore the effect of  $|\mathbf{E}|$  on the phase factor  $\phi_m + \Phi_m$  for a fixed direction of the electric field.

## Supplemental Material for: “Electric field induced thermal Hall effect of triplons in the quantum dimer magnets $X\text{CuCl}_3$ ( $X = \text{Tl}, \text{K}$ )”

### I. SYMMETRY ANALYSIS

#### A. Crystal structure and transformation property of spins under the symmetry

$X\text{CuCl}_3$  ( $X = \text{Tl}, \text{K}$ ) has a monoclinic crystal structure with space group  $P2_1/c$  [2, 8–10]. This space group has four kinds of symmetry operations,  $E$ ,  $I(0, 0, 0)$ ,  $2_1(b : 0, *, -1/4)$ , and  $c(-b/4)$  apart from Bravais lattice translations [see Fig. S1]. We consider the transformation property of spins under  $I(0, 0, 0)$ ,  $2_1(b : 0, *, -1/4)$ , and  $c(-b/4)$ . Let us denote by  $S_{\mu,l/r}^m(\mathbf{R})$  the  $\mu(= x, y, z)$  component of the left/right spin of the dimer in the unit cell at the position  $\mathbf{R}$  on the sublattice  $m$  ( $\{\mathbf{R}, m\}$ ). The spins are transformed under  $I(0, 0, 0)$  as follows:

$$I(0, 0, 0) : \begin{cases} S_{\mu,l/r}^1(\mathbf{R}) \rightarrow S_{\mu,r/l}^1(\mathbf{R}) \\ S_{\mu,l/r}^2(\mathbf{R}) \rightarrow S_{\mu,r/l}^2(\mathbf{R} + 2\hat{a} + \hat{b} + \hat{c}) \end{cases} \quad (\text{S1})$$

Since  $I(0, 0, 0)$  is the inversion operation, the spins do not change sign. The symmetry operation  $2_1(b : 0, *, -1/4)$  corresponds to a  $\pi$  rotation about an axis parallel to  $\hat{b}(z)$  and a half translation along the axis. Therefore, two of the three components of the spins change sign:

$$2_1(b : 0, *, -1/4) : \begin{cases} S_{\mu,l/r}^1(\mathbf{R}) \rightarrow \delta_\mu S_{\mu,r/l}^2(\mathbf{R} + \hat{a} + \hat{b}) \\ S_{\mu,l/r}^2(\mathbf{R}) \rightarrow \delta_\mu S_{\mu,r/l}^1(\mathbf{R} + \hat{a}) \end{cases}, \quad (\text{S2})$$

where  $\delta_x = \delta_y = -1$  and  $\delta_z = 1$ . The symmetry operation  $c(-b/4)$  represents a reflection through a glide plane perpendicular to  $\hat{b}(z)$  axis and a half translation along the  $c$  axis. Hence, two of three components of the spins change sign:

$$c(-b/4) : \begin{cases} S_{\mu,l/r}^1(\mathbf{R}) \rightarrow \delta_\mu S_{\mu,l/r}^2(\mathbf{R} + \hat{a} + \hat{c}) \\ S_{\mu,l/r}^2(\mathbf{R}) \rightarrow \delta_\mu S_{\mu,l/r}^1(\mathbf{R} - \hat{a}) \end{cases}, \quad (\text{S3})$$

#### B. The relative signs of the inter-dimer DM vectors

We can determine the relative signs of the inter-dimer DM vectors using Eqs. (S1), (S2), and (S3). The inter-dimer DM interaction term (3) is given as

$$\sum_{\eta=0,1} D_r^{\text{int}}(\eta(2\hat{a} + \hat{c}))\hat{z} \cdot [\mathbf{S}_r^1(\mathbf{R}) \times \mathbf{S}_r^2(\mathbf{R} + \eta(2\hat{a} + \hat{c}))] + D_l^{\text{int}}(\hat{b} + \eta(2\hat{a} + \hat{c}))\hat{z} \cdot [\mathbf{S}_l^1(\mathbf{R}) \times \mathbf{S}_l^2(\mathbf{R} + \hat{b} + \eta(2\hat{a} + \hat{c}))], \quad (\text{S4})$$

where  $D_\alpha^{\text{int}}(\mathbf{d}) = |\mathbf{D}_\alpha^{\text{int}}(\mathbf{d})|$ . Here, we note that the Hamiltonian is unchanged under the symmetry operation. Applying  $I(0, 0, 0)$ , we find

$$D_r^{\text{int}}(\mathbf{0}) = D_l^{\text{int}}(2\hat{a} + \hat{b} + \hat{c}). \quad (\text{S5})$$

while applying  $2_1(b : 0, *, -1/4)$ ,  $c(-b/4)$ , and translations, we find

$$D_r^{\text{int}}(\mathbf{0}) = -D_l^{\text{int}}(\hat{b}), \quad (\text{S6})$$

and

$$D_r^{\text{int}}(\mathbf{0}) = -D_r^{\text{int}}(2\hat{a} + \hat{c}). \quad (\text{S7})$$

The obtained results are expressed in Fig. 1 (b) in the main text.

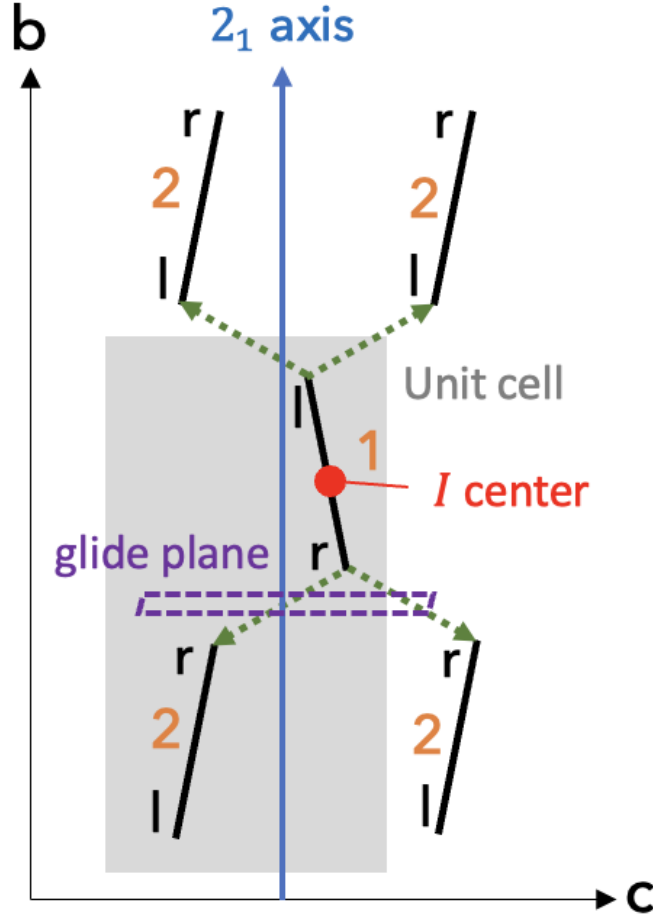


FIG. S1. A schematic picture of symmetries in  $\text{XCuCl}_3$  in the  $b$ - $c$  plane. The gray rectangle indicates the structural unit cell. The dotted green arrows indicate the sign convention for  $\mathbf{D}^{\text{int}}$ . The red point represents the inversion center, which is centered at each dimer. The solid blue arrow indicates the  $2_1$  spiral axis parallel to the  $\hat{b}(z)$  axis. The purple rhombus indicates the glide plane perpendicular to the  $\hat{b}(z)$  axis.

### C. Derivation of Eqs. (6) and (7)

Here, we derive Eqs. (6) and (7) in the main text. The local polarization on dimers  $\{\mathbf{R}, m\}$  is expressed using the polarization tensor and the left and right spins of the dimer [11–14, 65]

$$\mathbf{P}^m(\mathbf{R}) = \tilde{C}^m(S_l^m(\mathbf{R}) \times S_r^m(\mathbf{R})). \quad (\text{S8})$$



Also, the local polarization on dimers  $\{\mathbf{R}, m\}$  are transformed under  $I(0, 0, 0)$ ,  $2_1(b : 0, *, -1/4)$ , and  $c(-b/4)$  as follows:

$$I(0, 0, 0) : \begin{cases} P_\mu^1(\mathbf{R}) \rightarrow -P_\mu^1(\mathbf{R}) \\ P_\mu^2(\mathbf{R}) \rightarrow -P_\mu^2(\mathbf{R} + 2\hat{a} + \hat{b} + \hat{c}) \end{cases}, \quad (\text{S9})$$

$$2_1(b : 0, *, -1/4) : \begin{cases} P_\mu^1(\mathbf{R}) \rightarrow \delta_\mu P_\mu^2(\mathbf{R} + \hat{a} + \hat{b}) \\ P_\mu^2(\mathbf{R}) \rightarrow \delta_\mu P_\mu^1(\mathbf{R} + \hat{a}) \end{cases}, \quad (\text{S10})$$

$$c(-b/4) : \begin{cases} P_\mu^1(\mathbf{R}) \rightarrow -\delta_\mu P_\mu^2(\mathbf{R} + \hat{a} + \hat{c}) \\ P_\mu^2(\mathbf{R}) \rightarrow -\delta_\mu P_\mu^1(\mathbf{R} - \hat{a}) \end{cases}, \quad (\text{S11})$$

where  $\delta_x = \delta_y = -1$ , and  $\delta_z = 1$ . We can determine how the polarization tensor  $\tilde{C}^m$  is transformed under the symmetry operation by the above equations.

Applying  $I(0, 0, 0)$ , we find that there are no symmetry constraints on the elements of the polarization tensor  $\tilde{C}^m$  using Eqs. (S1), (S8), and (S9). Thus, we can express the polarization tensor of the sublattice 1 by nine independent components  $C_{\mu\nu}^1 (\mu, \nu = x, y, z)$  [11–14, 65]

$$\tilde{C}^1 = \begin{pmatrix} C_{xx}^1 & C_{xy}^1 & C_{xz}^1 \\ C_{yx}^1 & C_{yy}^1 & C_{yz}^1 \\ C_{zx}^1 & C_{zy}^1 & C_{zz}^1 \end{pmatrix}. \quad (\text{S12})$$

while applying  $2_1(b : 0, *, -1/4)$ ,  $c(-b/4)$ , and translations, we can obtain the matrix expression of the polarization tensor  $\tilde{C}^2$  using  $C_{\mu\nu}^1$  in (S12) as

$$\tilde{C}^2 = \begin{pmatrix} -C_{xx}^1 & -C_{xy}^1 & C_{xz}^1 \\ -C_{yx}^1 & -C_{yy}^1 & C_{yz}^1 \\ C_{zx}^1 & C_{zy}^1 & -C_{zz}^1 \end{pmatrix}. \quad (\text{S13})$$

Here, we used Eqs. (S2), (S3), (S8), (S10), and (S11). By substituting Eqs. (S12), and (S13) into Eq. (5), we can obtain Eq. (6) in the main text.

## II. THE EXPLICIT EXPRESSION OF THE CONSTANT TERM AND THE VARIATIONAL EQUATIONS

Here, we give the explicit expression of  $\mathcal{H}^{(0)}$  and the variational equations. The constant term  $\mathcal{H}^{(0)}$  is expressed as

$$\begin{aligned} \mathcal{H}^{(0)} = & -\frac{3J}{2} + \left( J - g\mu_B H - \frac{J_1 + J_2}{2} \right) (\sin^2 \theta_1 + \sin^2 \theta_2) + \frac{3(J_1 + J_2)}{4} (\sin^4 \theta_1 + \sin^4 \theta_2) \\ & + J_3 (\sin^2 \theta_1 \sin^2 \theta_2 + 2 \cos(\phi_2 - \phi_1) \sin \theta_1 \cos \theta_1 \sin \theta_2 \cos \theta_2) \\ & + \frac{\sin \theta_1 \cos \theta_1}{\sqrt{2}} D^{\text{ext},1} \sin(\phi_1 + \Phi_1) + \frac{\sin \theta_2 \cos \theta_2}{\sqrt{2}} D^{\text{ext},2} \sin(\phi_2 + \Phi_2). \end{aligned} \quad (\text{S14})$$

In the above expression (S14),  $D^{\text{ext},m}$  ( $m = 1, 2$ ) is the absolute value of the electric field-induced intra-dimer DM vector projected on  $x$ - $y$  plane, and  $\Phi_m = \arctan(D_y^{\text{ext},m}/D_x^{\text{ext},m})$ . Also, the variational equations for  $\theta_1$  and  $\phi_1$ , which can be obtained by differentiation of the constant term (S14) are expressed as

$$\begin{aligned} \frac{\partial \mathcal{H}^{(0)}}{\partial \theta_1} = & 2(J - g\mu_B H) \sin \theta_1 \cos \theta_1 - (J_1 + J_2) \sin \theta_1 \cos \theta_1 + 3(J_1 + J_2) \sin^3 \theta_1 \cos \theta_1 \\ & + 2J_3 (\sin \theta_1 \cos \theta_1 \sin^2 \theta_2 + \cos(\phi_2 - \phi_1) \cos 2\theta_1 \sin \theta_2 \cos \theta_2) \\ & + \frac{\cos^2 \theta_1 - \sin^2 \theta_1}{\sqrt{2}} D^{\text{ext},1} \sin(\phi_1 + \Phi_1) \\ = & 0, \end{aligned} \quad (\text{S15})$$

$$\begin{aligned} \frac{\partial \mathcal{H}^{(0)}}{\partial \phi_1} &= 2J_3 \sin(\phi_2 - \phi_1) \sin \theta_1 \cos \theta_1 \sin \theta_2 \cos \theta_2 + \frac{\sin \theta_1 \cos \theta_1}{\sqrt{2}} D^{\text{ext},1} \cos(\phi_1 + \Phi_1) \\ &= 0. \end{aligned} \quad (\text{S16})$$

The variational equations for  $\theta_2$  and  $\phi_2$  can also be obtained by changing the sublattice index as  $1 \leftrightarrow 2$  in Eqs. (S15) and (S16).

### III. THE EXPLICIT EXPRESSION OF THE BDG HAMILTONIAN

Here, we give the explicit expression for the  $4 \times 4$  BdG Hamiltonian (12) in the main text as follows:

$$H_{\text{BdG}}(\mathbf{k}) = \begin{pmatrix} \Xi(\mathbf{k}) & \Pi(\mathbf{k}) \\ \Pi^*(-\mathbf{k}) & \Xi^*(-\mathbf{k}) \end{pmatrix}, \quad (\text{S17})$$

where

$$\begin{aligned} \Xi(\mathbf{k})(i, i) &= f_1(\theta_i) + f_2(\theta_i) + g_1(\theta_i) \cos(\mathbf{k} \cdot \mathbf{d}_1) + g_2(\theta_i) \cos(\mathbf{k} \cdot \mathbf{d}_2) + h(\theta_i) + F_i + H_{\text{DM}}(\theta_i, \phi_i), \\ \Xi(\mathbf{k})(1, 2) &= G(\theta_1, \theta_2, \phi_1, \phi_2) + G_z(\theta_1, \theta_2, \phi_1, \phi_2), \\ \Xi(\mathbf{k})(2, 1) &= G(\theta_2, \theta_1, \phi_2, \phi_1) - G_z(\theta_2, \theta_1, \phi_2, \phi_1), \end{aligned} \quad (\text{S18})$$

$$\begin{aligned} \Pi(\mathbf{k})(i, i) &= h_1(\theta_i) \cos(\mathbf{k} \cdot \mathbf{d}_1) + h_2(\theta_i) \cos(\mathbf{k} \cdot \mathbf{d}_2), \\ \Pi(\mathbf{k})(1, 2) &= H(\theta_1, \theta_2, \phi_1, \phi_2) + H_z(\theta_1, \theta_2, \phi_1, \phi_2), \\ \Pi(\mathbf{k})(2, 1) &= H(\theta_1, \theta_2, \phi_1, \phi_2) + H_z(\theta_1, \theta_2, \phi_1, \phi_2), \end{aligned} \quad (\text{S19})$$

$$\begin{aligned} h(\theta) &= (J - g\mu_B H) \cos 2\theta, \\ f_i(\theta) &= \frac{J_i}{2} (5 \sin^2 \theta \cos^2 \theta - \sin^4 \theta), \\ g_i(\theta) &= \frac{J_i}{2} [\sin^2 \theta \cos^2 \theta - (\sin^4 \theta + \cos^4 \theta)], \\ h_i(\theta) &= \frac{3J_i}{2} \sin^2 \theta \cos^2 \theta, \\ H_{\text{DM}}(\theta_i, \phi_i) &= -\sqrt{2} \sin \theta_i \cos \theta_i D^{\text{ext},i} \sin(\phi_i + \Phi_i), \end{aligned} \quad (\text{S20})$$

$$\begin{aligned} F_1 &= J_3 [-\sin 2\theta_1 \sin 2\theta_2 \cos(\phi_2 - \phi_1) + \cos^2 \theta_1 \sin^2 \theta_2 - \sin^2 \theta_1 \sin^2 \theta_2], \\ F_2 &= J_3 [-\sin 2\theta_1 \sin 2\theta_2 \cos(\phi_2 - \phi_1) + \cos^2 \theta_2 \sin^2 \theta_1 - \sin^2 \theta_1 \sin^2 \theta_2], \\ G(\theta_1, \theta_2, \phi_1, \phi_2) &= J_3 [\cos(\mathbf{k} \cdot \mathbf{d}_{3+}) + \cos(\mathbf{k} \cdot \mathbf{d}_{3-})] \left[ e^{i(\phi_2 - \phi_1)} \cos^2 \theta_1 \cos^2 \theta_2 + e^{i(\phi_1 - \phi_2)} \sin^2 \theta_1 \sin^2 \theta_2 + \frac{\sin 2\theta_1 \sin 2\theta_2}{4} \right], \\ G_z(\theta_1, \theta_2, \phi_1, \phi_2) &= \frac{iD^{\text{int}}}{2} [\cos(\mathbf{k} \cdot \mathbf{d}_{3+}) - \cos(\mathbf{k} \cdot \mathbf{d}_{3-})] [e^{i(\phi_2 - \phi_1)} \cos^2 \theta_1 \cos^2 \theta_2 - e^{i(\phi_1 - \phi_2)} \sin^2 \theta_1 \sin^2 \theta_2], \\ H(\theta_1, \theta_2, \phi_1, \phi_2) &= J_3 [\cos(\mathbf{k} \cdot \mathbf{d}_{3+}) + \cos(\mathbf{k} \cdot \mathbf{d}_{3-})] \left[ -e^{i(\phi_2 - \phi_1)} \cos^2 \theta_1 \sin^2 \theta_2 - e^{i(\phi_1 - \phi_2)} \cos^2 \theta_2 \sin^2 \theta_1 + \frac{\sin 2\theta_1 \sin 2\theta_2}{4} \right], \\ H_z(\theta_1, \theta_2, \phi_1, \phi_2) &= \frac{iD^{\text{int}}}{2} [\cos(\mathbf{k} \cdot \mathbf{d}_{3+}) - \cos(\mathbf{k} \cdot \mathbf{d}_{3-})] [e^{i(\phi_1 - \phi_2)} \sin^2 \theta_1 \cos^2 \theta_2 - e^{i(\phi_2 - \phi_1)} \cos^2 \theta_1 \sin^2 \theta_2], \end{aligned} \quad (\text{S21})$$

where  $\mathbf{k} \cdot \mathbf{d}_1 = \frac{k_x + k_y}{2}$ ,  $\mathbf{k} \cdot \mathbf{d}_2 = 2k_x$ ,  $\mathbf{k} \cdot \mathbf{d}_{3\pm} = k_z \pm k_x$ .

#### IV. SYMMETRY CONDITION FOR THE NONZERO BERRY CURVATURE

Here, we explain a symmetry condition for the nonzero Berry curvature. The Berry curvature becomes zero when the BdG Hamiltonian (12) has the following effective PT symmetry [26, 33]:

$$P^\dagger H_{\text{BdG}}^*(\mathbf{k})P = H_{\text{BdG}}(\mathbf{k}), \quad (\text{S22})$$

where  $P$  is a paraunitary matrix. When we take  $P$  as  $P = I_{2 \times 2} \otimes \sigma_x$  ( $I_{2 \times 2}$  is  $2 \times 2$  identity matrix,  $\sigma_x$  is  $x$  component of Pauli matrix), the above condition is satisfied if

$$\Xi^3(\mathbf{k}) = \Pi^3(\mathbf{k}) = 0, \quad \Pi^i \in \mathbb{R} \quad (i = 0, 1, 2), \quad (\text{S23})$$

where  $\Xi^i(\mathbf{k})$  and  $\Pi^i(\mathbf{k})$  are defined as

$$\begin{aligned} \Xi(\mathbf{k}) &= \Xi^0(\mathbf{k})I_{2 \times 2} + \sum_{n=1}^3 \Xi^n(\mathbf{k})\sigma_n \\ \Pi(\mathbf{k}) &= \Pi^0(\mathbf{k})I_{2 \times 2} + \sum_{n=1}^3 \Pi^n(\mathbf{k})\sigma_n, \end{aligned} \quad (\text{S24})$$

where  $\Xi(\mathbf{k})$  and  $\Pi(\mathbf{k})$  represent the hopping and the pairing terms of the BdG Hamiltonian (S17), and  $\sigma_n$  ( $n = 1, 2, 3$ ) are Pauli matrices.

Then we apply the above symmetry condition for the present case in the following. Before applying the electric field, the variational parameters in Eq. (9) satisfy  $\theta_1 = \theta_2 \equiv \theta$  and  $\phi_1 - \phi_2 = \pm\pi$ . Hence, the BdG Hamiltonian (S17) satisfies the above condition (S23). However, after applying the electric field, the variational parameters  $\theta_m$  change from  $\theta$ , and we define the changes as  $\epsilon_m = \theta_m - \theta$ . To estimate the difference between the variational parameters  $\theta_2 - \theta_1$ , by subtracting the variational equations (S15) for  $\theta_1$  and  $\theta_2$  and keeping only terms first order in  $\epsilon_1$  and  $\epsilon_2$ , we can obtain the following equations

$$\theta_2 - \theta_1 = \epsilon_2 - \epsilon_1 \simeq \frac{D^{\text{ext},2} \sin(\phi_2 + \Phi_2) - D^{\text{ext},1} \sin(\phi_1 + \Phi_1)}{\sqrt{2}F(\theta)}, \quad (\text{S25})$$

$$F(\theta) = 2(J - g\mu_B H) - J_1 - J_2 + 3(J_1 + J_2) \frac{3 \sin^2 \theta \cos^2 \theta - \sin^4 \theta}{\cos^2 \theta - \sin^2 \theta} + 2J_3 \frac{\cos^2 \theta - 2 \sin^2 \theta - 4 \sin^2 \theta \cos^2 \theta}{\cos^2 \theta - \sin^2 \theta}. \quad (\text{S26})$$

From the above equation (S25), we can see that the electric field induced DM interaction term (5) gives rise to the difference between  $\theta_1$  and  $\theta_2$ . In this case, the symmetry condition (S23) is not satisfied, and thus the Berry curvature can be nonzero.

#### V. ELECTRIC FIELD DEPENDENCE OF THE BAND GAP

Here, we give the derivation of the electric field dependence of  $E_{\text{gap},\pm,j}(k_y)$ . The energy of the upper ( $n = 1$ ) and the lower ( $n = 2$ ) bands  $E_1$  and  $E_2$  at  $G_{\pm,j}$  can be written as

$$\begin{aligned} E_1 &= \sqrt{\xi_0^2 + \xi_3^2 - \pi_0^2 - \pi_3^2 + 2|\xi_0 \xi_3 - \pi_0 \pi_3|}, \\ E_2 &= \sqrt{\xi_0^2 + \xi_3^2 - \pi_0^2 - \pi_3^2 - 2|\xi_0 \xi_3 - \pi_0 \pi_3|}, \end{aligned} \quad (\text{S27})$$

where  $\xi_0$ ,  $\xi_3$ ,  $\pi_0$ , and  $\pi_3$  are defined as

$$\begin{aligned} \Xi &= \xi_0 I_{2 \times 2} + \xi_3 \sigma_3, \\ \Pi &= \pi_0 I_{2 \times 2} + \pi_3 \sigma_3, \end{aligned} \quad (\text{S28})$$

where  $\Xi$  and  $\Pi$  represent the hopping and the pairing terms of the BdG Hamiltonian (S17) at  $G_{\pm,j}$ ,  $I_{2 \times 2}$  is the  $2 \times 2$  identity matrix, and  $\sigma_n$  ( $n = 1, 2, 3$ ) are Pauli matrices. From the above equations (S27) and (S28), the band gap  $E_{\text{gap},\pm,j}$  is given as

$$E_{\text{gap},\pm,j}(k_y) = \frac{4|\xi_0 \xi_3 - \pi_0 \pi_3|}{E_1 + E_2}. \quad (\text{S29})$$

Also, approximate expressions for  $\xi_3$  and  $\pi_3$  at  $G_{\sigma,j}$  are given as

$$\begin{aligned}\xi_3 &\simeq v + t_1 \cos\left(\frac{j\pi}{2} - \sigma\frac{\pi}{4} + \frac{k_y}{2}\right)\sigma t_2, \\ \pi_3 &\simeq u_1 \cos\left(\frac{j\pi}{2} - \sigma\frac{\pi}{4} + \frac{k_y}{2}\right)\sigma u_2,\end{aligned}\tag{S30}$$

where  $\sigma = \pm$ ,  $j = 0, 1$ , and

$$\begin{aligned}v &= -2[(J_1 + J_2)(5 \sin \theta \cos \theta (\cos^2 \theta - \sin^2 \theta) - 2 \sin^3 \theta \cos \theta) - 2J_3 \sin^3 \theta \cos \theta - 4(J - g\mu_B H) \sin \theta \cos \theta](\epsilon_2 - \epsilon_1) \\ &\quad + \sqrt{2}(D^{\text{ext},2} \sin(\phi_2 + \Phi_2) - D^{\text{ext},1} \sin(\phi_1 + \Phi_1)) \sin \theta \cos \theta, \\ t_{1,2} &= 6J_{1,2}(\cos^2 \theta - \sin^2 \theta) \sin^2 \theta \cos^2 \theta (\epsilon_2 - \epsilon_1), \\ u_{1,2} &= \frac{3J_{1,2}}{2} \sin 2\theta \cos 2\theta.\end{aligned}\tag{S31}$$

In the above expressions,  $\theta$  is the variational parameter in the system without the electric field, and  $\epsilon_m = \theta_m - \theta$  ( $m = 1, 2$ ). From Eqs. (S25), (S26), (S30), and (S31), we find that  $\xi_3$  and  $\pi_3$  are proportional to  $D^{\text{ext},2} \sin(\phi_2 + \Phi_2) - D^{\text{ext},1} \sin(\phi_1 + \Phi_1)$ . In addition,  $\xi_0$  and  $\pi_0$  only depend on  $\theta$  when we keep only terms zero order in  $\epsilon_1$  and  $\epsilon_2$ . Therefore, from Eqs. (6), (S27), and (S29), we can see that  $E_{\text{gap},\pm,j}(k_y)$  is proportional to  $|\mathbf{E}|$  for a fixed direction of the electric field [77].